Signal-to-noise ratios in recorded patterned media

M.M. Aziz, B.K. Middleton and C.D. Wright

Abstract: The replay flux from isolated and sequences of recorded patterned elements was analysed and analytical expressions for the replay spectra were derived. The noise arising from bit size variations and bit position jitter has been modelled analytically allowing expressions for the signal-to-noise ratio for patterned media to be presented.

1 Introduction

Discrete patterned magnetic media have been suggested as an alternative to conventional continuous disk media for achieving high areal densities. This is mainly due to the reduced transition noise as compared to that from granular continuous media, and because of the improved thermal stability of the individual magnetic islands [1, 2]. Record and read-out measurements on patterned recording media with bit spacings as small as 70 nm (140 GBit/in^2) have been demonstrated using conventional magnetic heads [2] indicating the feasibility of using them to achieve high densities.

In previous work, the authors have derived expressions for the replay voltage and power spectral density from sequences of recorded magnetic islands [3]. These expressions included contributions of noise arising from variations in bit sizes and jitter in their positions. The aim of this paper is to generalise this theory by deriving expressions for the replay flux from isolated and arrays of recorded magnetic islands. This approach is more applicable to flux sensitive transducers which are more likely to be used with patterned media [2, 4]. Flux noise arising from the geometrical variations in the magnetic arrays is defined to separate the noise from the signal and to allow expressions for the noise power spectral densities to be derived. Ultimately, signal-to-noise ratios are calculated allowing the identification of the main parameters influencing the replay performance of recorded patterned media.

2 Head field function

The expressions derived in this paper are not limited to a specific type or geometry of replay transducer and are applicable to inductive, magnetoresistive [5], and magnetic force [6] type transducers. To use the single pole head as the replay element, the far-field approximations are used where the two-dimensional fields per unit current are given by [7]

$$H_x^p(x,\ y) = \frac{C\eta}{\pi}\frac{x}{(x^2+y^2)} \tag{1a}$$

$$H_y^p(x,\ y) = \frac{C\eta}{\pi}\frac{y}{(x^2+y^2)} \tag{1b}$$

where the replay head efficiency is η and there are C coil turns. Figure 1 indicates the geometry of the replay system where g is the pole length, y is the distance from the head surface, $\bar{x} = vt$ describes the position on the medium relative to the centre of the coordinate system, and v is the head-to-medium speed. The Fourier transforms of the x and y components of the head field are given, respectively, by $H_x^p(k,\ y) = -jC\eta\mathrm{sgn}(k)\cdot e^{-ky}$ and $H_y^p(k,\ y) = C\eta\cdot e^{-ky}$ where sgn(.) is the Signum function, $k = 2\pi/\lambda$ is the wavenumber, and λ is the wavelength.

The far-field approximations to the head field permit simple expressions for the signal to be derived and, because there are no nulls in their Fourier transforms, help to highlight the spectral features in the replay spectra that are related to the geometrical aspects of the medium.

3 Replay flux

3.1 Single bits

As indicated in Fig. 1, the magnetic islands assume a rectangular shape with length l, thickness δ and width w. The flux linked with the replay coil can be found using the reciprocity principle [7]

$$\Phi(\bar{x}) = \mu_o \int_z \int_y \int_x \boldsymbol{M}(x,\ y,\ z)\cdot\boldsymbol{H}^p(x+\bar{x},\ y,\ z)dxdydz \tag{2}$$

where μ_o is the permeability of free space. The head field per unit current, $\boldsymbol{H_p}$, is defined by (1), and the magnetisation of individual islands is described by the vector $\boldsymbol{M} = M\cos\theta\,\hat{\boldsymbol{x}} + M\sin\theta\hat{\boldsymbol{y}}$ with magnitude M, and orientation θ as shown in Fig. 1. $\hat{\boldsymbol{x}}$ and $\hat{\boldsymbol{y}}$ are unit vectors in the x- and y-directions, respectively. Thus in two dimensions, (2) reduces to

$$\Phi(\bar{x}) = \alpha\mu_o M \int_{z=-w/2}^{w/2}\int_{y=d}^{d+\delta}\int_{x=-l/2}^{l/2} \{\cos\theta\cdot H_x^p(x+\bar{x},\ y) + \sin\theta\cdot H_y^p(x+\bar{x},\ y)\}\,dxdydz \tag{3}$$

where $\alpha = \pm 1$ indicates the direction of the magnetisation inside the magnetic elements. Evaluating the Fourier

IEE Proceedings online no. 20030865
doi:10.1049/ip-smt:20030865
Paper first received 11th February and in revised form 24th July 2003

M.M. Aziz and C.D. Wright are with the School of Engineering, Computer Science and Mathematics, University of Exeter, Exeter EX4 4QF, UK
B.K. Middleton is with the Department of Computer Science, University of Manchester, Oxford Road, Manchester M13 9PL, UK

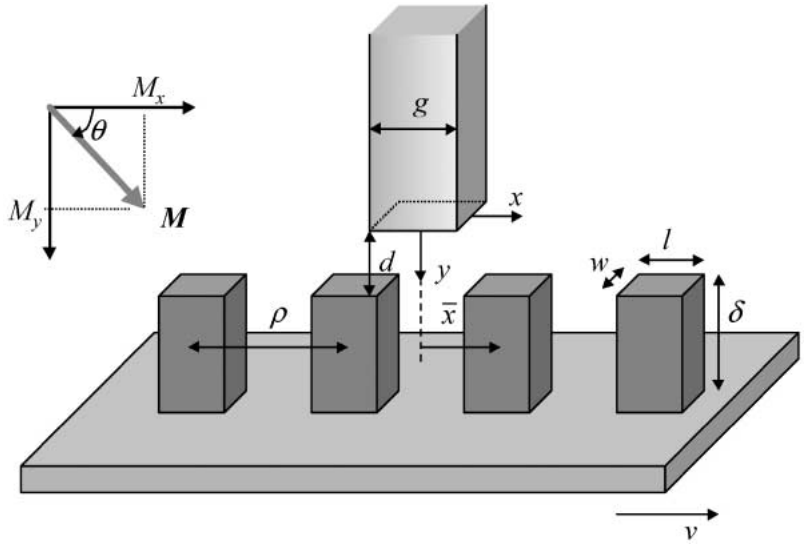

Fig. 1 *Geometry of replay system and magnetisation vector of individual magnetic islands*

transform of (3) yields

$$\Phi(k) = \alpha\mu_o M \int_{z=-w/2}^{w/2} \int_{y=d}^{d+\delta} \int_{x=-l/2}^{l/2} \{\cos\theta \cdot H_x^p(k, y)e^{jkx} + \sin\theta \cdot H_y^p(k, y)e^{jkx}\}\, dxdydz \quad (4)$$

With no soft magnetic underlayer, a volume integration of (4) yields the replay flux transform as

$$\Phi(k) = \alpha\mu_o M(wl\delta) \cdot (\sin\theta - j\,\mathrm{sgn}(k)\cos\theta)[H_s(k)] \cdot \left[\frac{\sin(kl/2)}{(kl/2)}\right] \cdot [e^{-kd}] \cdot \left[\frac{1 - e^{-k\delta}}{k\delta}\right] \quad (5)$$

$H_s(k)$ is the Fourier transform of the surface field ($y = 0$) and is equal to the constant $C\eta$ in this case, but can represent the gap loss function of a given transducer geometry. Equation (5) is plotted in Fig. 2 where a null in the spectrum at a wavelength equal to the bit length l can be observed. This null results from the term $\sin(kl/2)/(kl/2)$ in (5) and implies that in addition to the replay gap nulls produced by real heads, the read-out resolution in patterned media is further limited by the length of the magnetic islands.

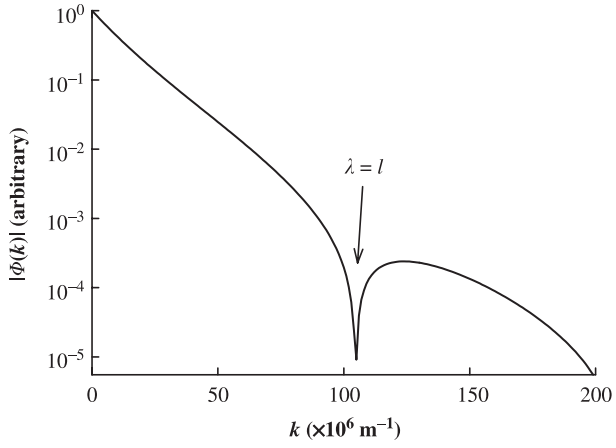

Fig. 2 *Replay spectrum for an isolated magnetic island having length 60 nm, width 60 nm, thickness 120 nm, 30 nm head-to-medium spacing*

3.2 Multiple bits

For an infinite sequence of vertically magnetised islands and separated by a distance ρ between their centres as shown in Fig. 1, the replay flux can be written as the superposition of the flux from isolated magnetic islands in the form

$$\Phi_s(\bar{x}) = \sum_{n=-\infty}^{\infty} \Phi(\bar{x} - n\rho) \quad (6)$$

Taking the Fourier transform of (6) yields

$$\Phi_s(k) = k_o\Phi(k) \sum_{n=-\infty}^{\infty} \delta(k - nk_o) \quad (7)$$

where $k_o = 2\pi/\rho$. As shown in Fig. 3 the spectrum of an infinite sequence of recorded bits is a sequence of Dirac delta functions occurring at spatial frequencies nk_o and whose magnitude is weighted by Fourier transform of the isolated bit.

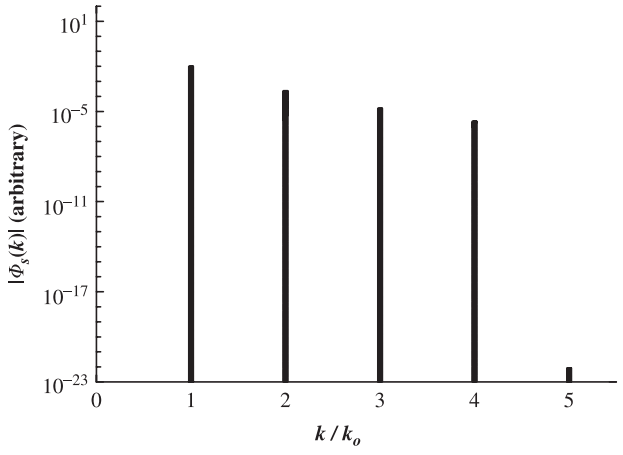

Fig. 3 *Replay spectrum for an infinite sequence of vertically magnetised islands spaced 100 nm between their centres and having the same dimensions as in Fig. 2.*

Following from (7), the peak value of the fundamental component ($n = 1$) of the replay flux, including positive and negative wavenumbers, is given by

$$\Phi^{fund}(k_o) = 2k_o\Phi(k_o) \quad (8)$$

4 Flux noise

Noise in patterned media is mainly caused by the finite tolerances in the fabrication method employed in producing the magnetic arrays. This noise is modelled as random variations in bit sizes and jitter in the bit positions.

Including position jitter, s, the replay flux for an infinite sequence of vertically magnetised bits can be written as

$$\Phi_s(\bar{x}) = \sum_{n=-\infty}^{\infty} \Phi(\bar{x} - n\rho - s_n)$$

which for small perturbations in s_n, can be expanded to the first-order Taylor series

$$\Phi_s(\bar{x}) = \sum_{n=-\infty}^{\infty} \Phi(\bar{x} - n\rho) + \sum_{n=-\infty}^{\infty} s_n \frac{\partial \Phi(\bar{x} - n\rho)}{\partial \bar{x}} \tag{9}$$

In the following analysis, the flux noise arising from individual magnetic islands will be defined as

$$\Phi^N(\bar{x}) = \Phi(\bar{x}) - \overline{\Phi(\bar{x})} \tag{10}$$

where $\Phi(\bar{x})$ is the replay flux including noise, and $\overline{\Phi(\bar{x})}$ is the mean (noiseless) replay flux signal as given by (3). The noise power spectral density is then given by [8]

$$S(k) = \lim_{L\to\infty} \frac{1}{L} \overline{\left| \sum_{n=-\infty}^{\infty} \Phi_n^N(k) \right|^2} \tag{11}$$

where the overbar indicates spatial averages and L is the averaging interval. To evaluate the noise power spectral density in (11), a number of assumptions are made: first, the magnetic islands are uncorrelated and therefore the noise will be limited in extent by the bit spacing ρ; secondly, noise sources are uncorrelated; and finally, position jitter follows a Gaussian distribution with a mean value of zero. According to these assumptions the noise power spectral density was evaluated to be

$$S(k) = \frac{1}{\rho}\{\overline{|\Phi(k)|^2} \cdot (1 + k^2\overline{s^2}) - \overline{|\Phi(k)|}^2\} \tag{12}$$

where $\Phi(k)$ is given by (5). From (12) it can be seen that the noise power spectral density increases with reduced bit spacing. This is expected since reducing the bit spacing increases the proportion of the 'noisy' magnetic bit regions at the expense of the 'noiseless' nonmagnetic regions.

Random variations in the thicknesses of the magnetic islands lead to fluctuations in the head-to-medium spacing. As a result, the lower limit of integration with respect to y in (4) is changed to the random variable d_r to account for this fluctuation which has a mean value of $\bar{d}$. The upper integration limit is, however, maintained at $d+\delta$ since changes in δ cause equal changes in d in the opposite direction thus keeping the sum $d+\delta$ constant. Substituting from (5) and with $\alpha = 1$, (12) becomes

$$S(k) = \frac{\mu_o^2 |H_s(k)|^2}{\rho} \left\{ \overline{M^2} \cdot \overline{w^2} \cdot \left[\frac{\sin^2(kl/2)}{(k/2)^2} \right] \right.$$
$$\left[\frac{\overline{e^{-2kd_r}} - 2\overline{e^{-kd_r}} e^{-k(\bar{d}+\delta)} + e^{-2k(\bar{d}+\delta)}}{k^2} \right] \cdot [1 + k^2\overline{s^2}]$$
$$\left. -\bar{M}^2 \cdot \bar{w}^2 \left[\frac{\sin^2(k\bar{l}/2)}{(k/2)^2} \right] \cdot [e^{-2k\bar{d}}] \cdot \left[\frac{(1 - e^{-k\bar{\delta}})^2}{k^2} \right] \right\} \tag{13}$$

In previous work [3], in analyses of SEM and AFM images of PtCo patterned samples it was found that the variations in bit length, width and thickness follow closely the Gaussian distribution

$$g(r) = \frac{1}{\sigma\sqrt{2\pi}} e^{-(r-m)^2/(2\sigma^2)} \tag{14}$$

with mean m and standard deviation σ.

Evaluation of the averages in (13) according to

$$\overline{f(r)} = \int_{r=-\infty}^{\infty} f(r)g(r)dr$$

using the distribution in (14), yields the replay flux noise power spectral density, which can be written in the form

$$S(k) = \frac{\mu_o^2 |H_s(k)|^2 (\bar{l}\bar{w}\bar{\delta})^2}{\rho} [e^{-2k\bar{d}}] \cdot \left[\frac{\sin(k\bar{l}/2)}{k\bar{l}/2} \right]^2 \left[\frac{1 - e^{-k\bar{\delta}}}{k\bar{\delta}} \right]^2$$
$$\left\{ \overline{M^2} \left(1 + \frac{\sigma_w^2}{\bar{w}^2} \right) \cdot \left(\frac{1 - \cos(k\bar{l}) e^{-k^2\sigma_l^2/2}}{1 - \cos(k\bar{l})} \right) \cdot (1 + k^2\sigma_s^2) \cdot \right.$$
$$\left. \left(\frac{e^{2k^2\sigma_d^2} - 2e^{k^2\sigma_d^2/2} e^{-k\bar{\delta}} + e^{-2k\bar{\delta}}}{1 - 2e^{-k\bar{\delta}} + e^{-2k\bar{\delta}}} \right) - \bar{M}^2 \right\} \tag{15}$$

where σ_w, σ_l, σ_d, and σ_s are the standard deviations of the bit width, length, position jitter and head-to-medium spacing, respectively. The terms in square brackets represent the replay losses.

The noise power spectral density in (15) is plotted in Fig. 4 to illustrate the effect of jitter noise alone on the noise spectrum, with all the other noise variances set to zero. It can be seen that jitter noise mainly influences the short wavelength part of the noise spectrum and its magnitude increases with increasing jitter variance. Jitter noise has little effect at very long wavelengths.

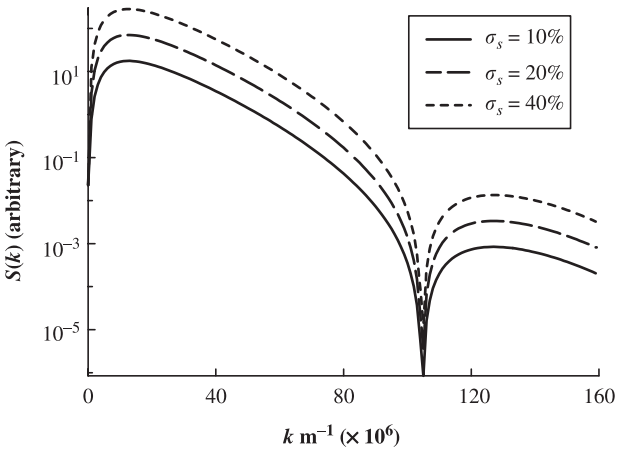

Fig. 4 *Noise power spectral densities for jitter noise only with increasing jitter noise variance. Bit size and head-to-medium spacing as in Fig. 2. The standard deviation is shown as a percentage of the bit spacing, 100 nm*

Figure 5 is obtained by setting the position jitter variance to zero in (15) and shows that bit size variations are mainly a long wavelength phenomenon and the noise power increases with increasing variance particularly at short wavelengths.

The combined effect of bit size variation and position jitter on the flux noise power spectral density is demonstrated in Fig. 6, which illustrates how size variations cause the disappearance of the spectral null corresponding to the bit length.

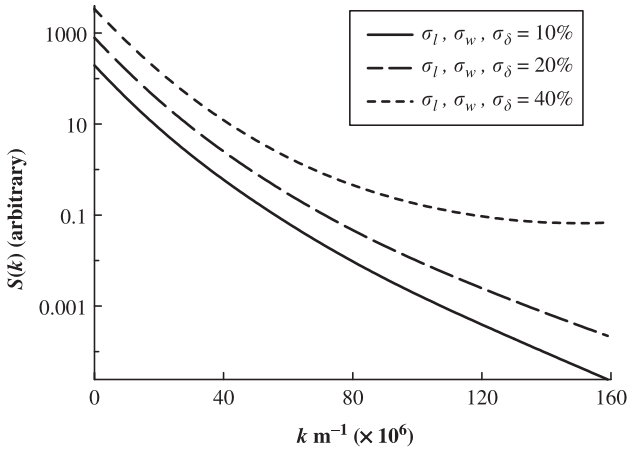

Fig. 5 *Noise power spectral densities for bit size variation only. The standard deviation is a percentage of the bit length (60 nm), width (60 nm) and thickness (120 nm)*

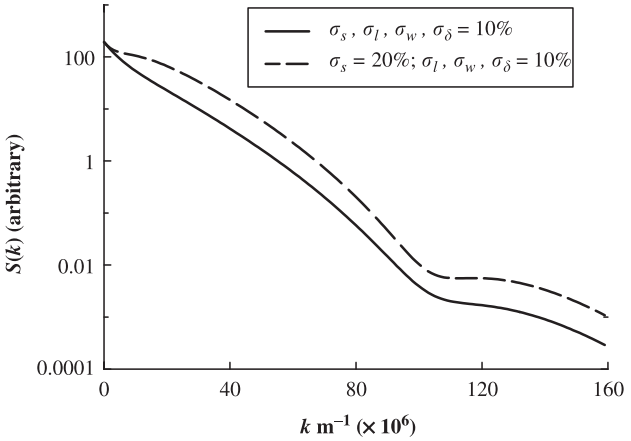

Fig. 6 *Noise power spectral density including bit position jitter and bit size variations*

5 Signal-to-noise ratios

The signal-to-noise ratio (SNR) is defined as the ratio of the peak signal power to the slot noise power at the fundamental wavenumber $k_o = 2\pi/\rho$ [9]

$$SNR = \frac{|\Phi^{fund}(k_o)|^2}{NP(k_o)} \tag{16}$$

where Φ^{fund} is given by (8), and NP is the noise power of positive and negative wavenumbers in a bandwidth Δk and is given by

$$NP(k) = 2S(k)\Delta k \tag{17}$$

Assuming the same magnetisation for all elements such that $\bar{M}^2 = \overline{M^2}$, and noting that $l = \bar{l}$, $w = \bar{w}$, $\delta = \bar{\delta}$, and $d = \bar{d}$, the SNR can be derived from (5), (15) and (16) as

$$SNR = 4\pi k_o \left\{ \left[\left(1 + \frac{\sigma_w^2}{\bar{w}^2}\right) \cdot \left(\frac{1 - \cos(k\bar{l}) e^{-k^2\sigma_l^2/2}}{1 - \cos(k\bar{l})} \right) \right. \right.$$
$$\left. \left. (1 + k^2\sigma_s^2) \left(\frac{e^{2k^2\sigma_d^2} - 2e^{k^2\sigma_d^2/2} e^{-k\bar{\delta}} + e^{-2k\bar{\delta}}}{1 - 2e^{-k\bar{\delta}} + e^{-2k\bar{\delta}}} \right) - 1 \right] \Delta k_o \right\}^{-1} \tag{18}$$

It is clear from the above that there will be noise at all wavelengths caused by element width variations and that position jitter noise disappears at very long wavelengths but grows as wavelengths shorten. The long and short wavelength limits of noise and SNR will now be discussed.

5.1 Long wavelengths

The noise power spectral density in the limit of long wavelengths ($k \to 0$) can be evaluated by taking the first terms in the expansion of k around 0 in (15) to obtain

$$S(k) = \frac{\mu_o^2 |H_s(k)|^2 (\bar{l}\bar{w}\bar{\delta})^2}{\rho} \left\{ \overline{M^2} \left(1 + \frac{\sigma_w^2}{\bar{w}^2}\right) \left(1 + \frac{\sigma_l^2}{\bar{l}^2}\right) \left(1 + \frac{\sigma_d^2}{\bar{\delta}^2}\right) - \bar{M}^2 \right\} \tag{19}$$

Noting that $\sigma_d^2 = \sigma_\delta^2$ (because $\bar{d} + \bar{\delta}$ is constant) and using (17), the noise power becomes

$$NP(k) = \frac{2\mu_o^2 |H_s(k)|^2 (\bar{l}\bar{w}\bar{\delta})^2}{\rho} \left\{ \overline{M^2} \left(1 + \frac{\sigma_w^2}{\bar{w}^2}\right) \left(1 + \frac{\sigma_l^2}{\bar{l}^2}\right) \left(1 + \frac{\sigma_\delta^2}{\bar{\delta}^2}\right) - \bar{M}^2 \right\} \Delta k \tag{20}$$

With the same magnetisation in each element and assuming that all variances are small, (20) reduces to

$$NP(k) = \frac{2\mu_o^2 |H_s(k)|^2 (\bar{l}\bar{w}\bar{\delta})^2 \bar{M}^2}{\rho} \left\{ \frac{\sigma_w^2}{\bar{w}^2} + \frac{\sigma_l^2}{\bar{l}^2} + \frac{\sigma_\delta^2}{\bar{\delta}^2} \right\} \Delta k \tag{21}$$

and the SNR at k_o becomes

$$SNR = \frac{4\pi k_o}{\left(\frac{\sigma_w^2}{\bar{w}^2} + \frac{\sigma_l^2}{\bar{l}^2} + \frac{\sigma_\delta^2}{\bar{\delta}^2} \right) \Delta k_o} \tag{22}$$

Equation (22) shows that when the magnetic islands are far apart, the main noise contribution is primarily due to bit dimension variations.

5.2 Short wavelengths

The SNR as indicated by (18) can be expanded for small values of the variances and at short wavelengths (large k) can be approximated by

$$SNR = \frac{4\pi k_o}{\left(\frac{\sigma_w^2}{\bar{w}^2} + \frac{k_o^2 \sigma_l^2 \cos(k_o\bar{l})}{2(1 - \cos(k_o\bar{l}))} + k_o^2\sigma_s^2 + 2k_o^2\sigma_\delta^2 \right) \Delta k_o} \tag{23}$$

This shows that the variances in element length and thickness in conjunction with element position jitter will predominate.

6 Conclusions

General expressions for the replay signal and noise from recorded patterned media were derived. Variations in bit width, length and thickness are present at all wavelengths but position jitter contributes little at long wavelengths and strongly at short wavelengths. All the variances studied here place considerable demands on the requirements for uniformity in the shapes and positions of storage elements in patterned recording media.

7 Acknowledgment

The authors are indebted to Dr P. W. Nutter for providing the images of the patterned magnetic arrays for the early part of this work.

8 References

1 White, R. I., New, R.M., and Pease, F.W.: 'Patterned media: a viable route to 50 GBit/in^2 and up for magnetic recording?', *IEEE Trans. Magn.*, 1997, **33**, pp. 990–995

2 Rettner, C.T., Anders, S., Thomson, T., Albrecht, M., Ikeda, Y., Best, M.E., and Terris, B.D.: 'Magnetic characterization and recording properties of patterned $Co_{70}Cr_{18}Pt_{12}$ perpendicular media', *IEEE Trans. Magn.*, 2002, **38**, pp. 1725–1730

3 Aziz, M.M., Wright, C.D., Middleton, B.K., Du, H., and Nutter, P.W.: 'Signal and noise characteristics of patterned media', *IEEE Trans. Magn.*, 2002, **38**, pp. 1964–1966

4 Hughes, G.F.: 'Read channels for patterned media', *IEEE Trans. Magn.*, 1999, **35**, pp. 2310–2312

5 Shtrikman, S., and Smith, D.R.: 'Analytical formulas for the unshielded magnetoresistive head', *IEEE Trans. Magn.*, 1996, **32**, pp. 1987–1994

6 Wright, C.D., and Hill, E.W.: 'A reciprocity-based approach to understanding magnetic force microscopy', *IEEE Trans. Magn.*, 1996, **32**, pp. 4144–4146

7 Middleton, B.K.: 'The recording and reproducing processes', *in* Mee, C.D. and Daniel, E.D. (Eds.), 'Magnetic recording technology' (McGraw-Hill, New York, 1996, 2nd Edn.)

8 Lathi, B.P.: 'Modern digital and analog communication systems' (Oxford University Press, New York, 1998, 3rd Edn.)

9 Bertram, H.N.: 'Theory of magnetic recording' (Cambridge University Press, London, 1994)